SLAC-TN-10-063

UCRL-TR-222642
LCLS-TN-06-10
July 12, 2006

The Gas Flow from the Gas Attenuator to the Beam Line*

D.D. Ryutov
Lawrence Livermore National Laboratory, Livermore, CA 94551

Abstract

The gas leak from the gas attenuator to the main beam line of the Linac Coherent Light Source has been evaluated, with the effect of the Knudsen molecular beam included. It has been found that the gas leak from the gas attenuator of the present design, with nitrogen as a working gas, does not exceed 10^{-5} *torr×l/s* even at the highest pressure in the main attenuation cell (20 *torr*).

* This work was performed under the auspices of the U.S. Department of Energy by University of California Lawrence Livermore National Laboratory under Contract W-7405-Eng-48.
Work supported in part by the DOE Contract DE-AC02-76SF00515. This work was performed in support of the LCLS project at SLAC.

The gas flow from the gas attenuator to the beam line

D.D. Ryutov

Lawrence Livermore National Laboratory, Livermore, CA 94551

Abstract

The gas leak from the gas attenuator to the main beam line has been evaluated, with the effect of the Knudsen molecular beam included. It has been found that the gas leak from the gas attenuator of the present design, with nitrogen as a working gas, does not exceed 10^{-5} *torr×l/s* even at the highest pressure in the main attenuation cell (20 *torr*).

The eventual measure of the effect of the gas attenuator on the vacuum conditions in the beam line is the amount of gas flowing out to the beam line through the end apertures of the gas attenuator. The general assessment of this issue has been provided in Refs. 1 and 2. Here I revisit this problem, concentrating on the currently accepted design of the gas attenuator with nitrogen as a working gas and the gas pressure in the differential pumping system as measured in the prototype of the attenuator (S. Shen and co-workers [3]). I specifically address an issue of the Knudsen molecular beam that emerges through the final aperture [1]. [Desirability of an explicit accounting for this effect for the current design was brought up by Dr. W. Stoeffl (LLNL) to whom I express my gratitude.] I find that the beaming effect is relatively insignificant in the currently accepted design (unlike in the much more ambitious design [1], where the size of the apertures was much bigger and the beaming was substantial [1]). We do not include in our analysis the possible presence of the gas detector (e.g., [4]) which may become an integral part of the gas attenuator [5]. The presence of the gas detector can be readily incorporated in the analysis if so desired.

In the further discussion we need the elastic scattering cross-section σ for N_2 molecules. The data in the literature vary by a factor of ~ 2. We will take some "median" value (see Ref. [6], p. 302):

$$\sigma = 3\times 10^{-15} cm^2 . \qquad (1)$$

Some uncertainty in this number does not affect the final estimates in any significant manner.

The schematic of the differential pumping system is shown in Fig. 1. The cell "0" is the gas attenuator proper, whereas cells 1-3 are the stages of the differential pumping system. The cells are connected by orifices, all having the radius of

$$a = 0.15 \;\; cm . \qquad (2)$$

Pressures in the cells depend on the pump speed of the corresponding pumps. We will assume, as representative values, the pressures listed in Table 1 (based on the results by S. Shen et al. [3]). Assuming that the gas in all cells is at roughly the room temperature (see more details below), we relate the pressure and the density via an equation

$$n(cm^{-3}) = 3.5\times 10^{16}\, p(torr) . \qquad (3)$$

The collisional mean free path λ is related to the density and cross-section by:

$$\lambda = \frac{1}{n\sigma}. \qquad (4)$$

The gas density and mean free path are also presented in Table 1.

Table 1 Parameters of the gas attenuator

Cell number	0	1	2	3
Length *l*, cm	600	30	30	30
Pressure *p*, torr	20	1	3×10^{-3}	3×10^{-6}
Gas density *n*, cm^{-3}	7×10^{17}	3.5×10^{16}	1.05×10^{14}	1.05×10^{11}
m.f.p. λ,cm	4.8×10^{-4}	9.5×10^{-3}	3.1	3100

One sees that, in the cells “0” and “1”, the m.f.p. is much smaller than the orifice radius. So, the gas flow from cell “0” to “1” and from cell “1” to “2” is governed by hydrodynamic equations. The amount of gas flowing between these cells would weakly depend on the length of the channel connecting the cells, unless its length becomes quite large compared to the orifice radius.

The hydrodynamic flow in the channel reaches the local sonic speed and then becomes supersonic. The temperature in the flow drops because of the adiabatic expansion of the collisional gas. Then this jet rams into the gas that is confined in the adjacent cell, forming a shock wave and reheating the gas to the temperature comparable to the initial temperature. The flow structure is qualitatively illustrated by Fig. 2. The position of the shock is determined from the condition that the ram pressure of the incoming flow is equal to the thermal pressure of the shocked gas (see below). For the parameters listed in Table 1, the shock will be situated at a distance ~ 10 millimeters from the orifice.

To evaluate the parameters of the shock in a more quantitative fashion, we note that the gas flowing out of the cell “0” experiences a strong expansion and, therefore, the flow entering the shock is strongly supersonic. The shock, therefore, is a strong shock and the compression ratio can be determined from the equation [7]:

$$\frac{n_{post-shock}}{n_{pre-shock}} = \frac{\gamma+1}{\gamma-1} = 6 \qquad (5)$$

where γ is an adiabatic index equal to 7/5 for the diatomic gas. The post-shock density is the gas density n_1 in the cell “1”, so that the pre-shock density is (see Table 1):

$$n_{pre-shock} = n_1/6 = n_0/120 \qquad (6)$$

In other words, the gas flowing out of the cell “0” expands by a factor of 120 before entering the shock. So strong an expansion causes the cooling of the gas to the temperature

$$T_{pre-shock} = T_0 \left(\frac{n_{pre-shock}}{n_0} \right)^{\gamma-1} = 0.147 T_0 \approx 44 \ \ K \qquad (7)$$

The gas cooling in the pre-shock region may cause the gas condensation into molecular clusters, because the pre-shock temperature is well below the condensation temperature for nitrogen (this effect for xenon was briefly mentioned in Ref. [1]). On the other hand, the pre-shock density is quite low, and the transit time is short. Therefore, it is not clear whether the clusters actually form.

The flow velocity of the pre-shocked gas is approximately equal to [7]:

$$\mathrm{v}_{pre-shock} = s_0 \sqrt{\frac{2}{\gamma-1}} \qquad (8)$$

where

$$s_0 = \sqrt{\frac{\gamma k T_0}{m}} \qquad (9)$$

is the sound speed in the cell "0", with *k* being the Boltzmann constant, and *m* being the mass of the nitrogen molecule. The gas temperature behind the strong shock is [7]:

$$T_{post-shock} = \frac{m \mathrm{v}^2_{pre-shock}}{k} \frac{2(\gamma-1)}{(\gamma+1)^2} = T_0 \frac{4\gamma}{(\gamma+1)^2} = 0.97 T_0 \qquad (10)$$

So, indeed, the temperature of the shocked gas returns essentially to the initial temperature in the cell "0."

The temperature of the gas in the cell "1" may somewhat decrease because of the gas expansion caused by the pumping the gas out of the cell. An opposing effect would be the heat exchange with the walls in the strongly turbulent flow of the shocked gas.

The distance of the tip of the shock front from the orifice connecting cells "0" and "1" can be found by using Eqs. (5) and (11) of Ref. [2]. For the orifice radius of 1.5 mm, this distance is 13 mm.

The situation repeats itself in the cell 2, with the difference that now the mean-free path becomes relatively large, and the shock transition is much more smooth, occurring at the scale of order of 3 cm (the mean free path in the expanded gas). In addition to shock heating, the molecules on their way to the opposite end, experience at least several collisions with the side walls of the cell (as the mean free path is comparable with the cell radius). We conclude that the gas temperature in the cell 2 is of order of the room temperature.

Consider now the transition between cells 2 and 3. Here the mean-free path in the incoming gas is much larger than the orifice size. In the downstream cell (cell 3) it is much larger than even the cell length l_3. The flow through the orifice under such circumstances is a Knudsen flow which depends on the length of the channel. We consider the worst case where the length is much less than the orifice radius (the situation depicted in Fig. 3).

The particles experience the last collision at a distance $\sim \lambda$ from the orifice. From there on their motion is collisionless. The amount of gas coming through the orifice can be evaluated by throwing an isotropic "half-Maxwellian" distribution on it. To evaluate the role of the "beaming," we need to consider the particles that reach the orifice (A in Fig. 3) connecting the stage 3 with the undulator. The number of particles making it

through this last orifice is determined by the purely geometric considerations. For the Maxwellian distribution with the temperature T it is equal to

$$\dot{N} = a^2 \left(\frac{a}{l_3} \right)^2 n_2 \sqrt{\frac{2\pi kT}{m}} \tag{11}$$

where T is the temperature, m is the mass of the molecule, k is the Boltzmann constant, and l_3 is the length of cell 3. For nitrogen at T=300 K, this equation can be presented as

$$\dot{N}\left(\frac{particles}{s} \right) = 7{,}4 \times 10^4 [a(cm)]^2 \left(\frac{a}{l_3} \right)^2 n_2 (cm^{-3}) \tag{12}$$

or as

$$\dot{N}\left(\frac{particles}{s} \right) = 2.6 \times 10^{21} [a(cm)]^2 \left(\frac{a}{l_3} \right)^2 p_2 (torr) \tag{13}$$

or, equivalently, as

$$\dot{N}\left(\frac{torr \times l}{s} \right) = 74 [a(cm)]^2 \left(\frac{a}{l_3} \right)^2 p_2 (torr) . \tag{14}$$

For the parameters defined by Eq. (2) and Table 1, and l_3=30 cm, this yields $\dot{N} = 4.4 \times 10^{12} (particles/s)$ or $\dot{N} = 1.25 \times 10^{-7} (torr \times l/s)$. These particles form a well-collimated beam in the upstream vacuum volume, with the divergence (a/l_3)~5 mrad. It will expand to the radius of 3 cm and hit the walls of the vacuum pipe at a distance ~ 6 m from the orifice. The beam broadening will be also assisted by the intra-beam scattering, because the particles in the beam have Maxwellian distribution over the parallel velocity, with the temperature T. Note a strong dependence of the beam component on the orifice radius (~a^4). This is exactly the reason that lead the authors of Ref. [1] (where a was assumed to be 0.5 cm, see Sec. 3 of Ref. 1) to the conclusion that the molecular beam escaping to the main accelerator volume is very strong and should be further attenuated by a Penning discharge cell. In the present design the beam component is much weaker.

The vast majority of the particles entering the 3rd cell from the 2nd cell hit the walls of the 3rd cell and get scattered. These are the particles that are responsible for the density n_3 mentioned in Table 1. They also contribute to the gas flow to the undulator. This component of the gas outflow is, obviously,

$$\dot{N}' = a^2 n_3 \sqrt{\frac{2\pi kT}{m}} . \tag{15}$$

The prime is used to distinguish the "quasi-isotropic" component from the "beam" component. For n_3 as in Table 1, this is $\dot{N}' = 1.74 \times 10^{14} (particles/s)$, or $\dot{N}' = 5 \times 10^{-6} (torr \times l/s)$. In other words, the "quasi-isotropic" component is 40 times larger than the "beam" component.

Acknowledgments

The author is grateful to R. Bionta, S. Shen, and the whole LCLS XTOD group for helpful discussions.

References

1. D.D. Ryutov, A. Toor. “X-ray attenuation cell,” LCLS Technical Note 00-10, May 2000.
2. D.D. Ryutov, R.M. Bionta, M.A. McKernan, S. Shen, J.W. Trent. “The physics analysis of the gas attenuator with argon as a working gas,” LCLS Technical Note 06-1, January 2006.
3. S. Shen. Presentation to LCLS FAC Meeting, October 27, 2006.
4. D.D. Ryutov, R.M. Bionta, S. Hau-Riege. “Photoluminescence for non-destructive total energy measurements and imaging of X-ray beam in the Linac Coherent Light Source,” UCRL-TR-220017-DRAFT, March 2006.
5. S. Shen. Presentation to the LCLS SCR Committee. June 27, 2006.
6. I.K. Kikoin (Ed.). “Tables of Physical Quantities” (Moscow, Atomizdat, 1976), in Russian.
7. L.D. Landau, E.M. Lifshitz. Fluid Mechanics (Oxford, Pergamon Press), 1987.

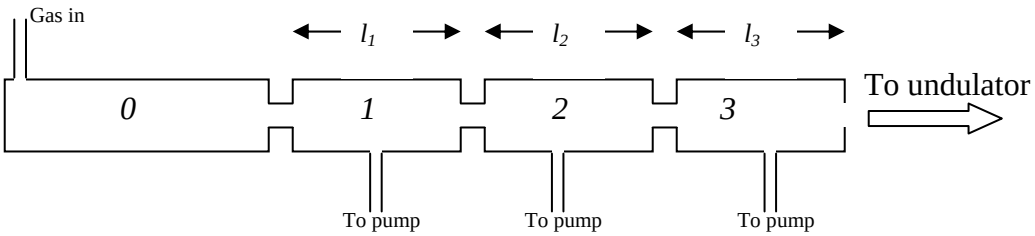

Fig. 1 Sketch of the differential pumping system. The actual system is left-right symmetric with respect to the equatorial plane situated near the gas inlet.

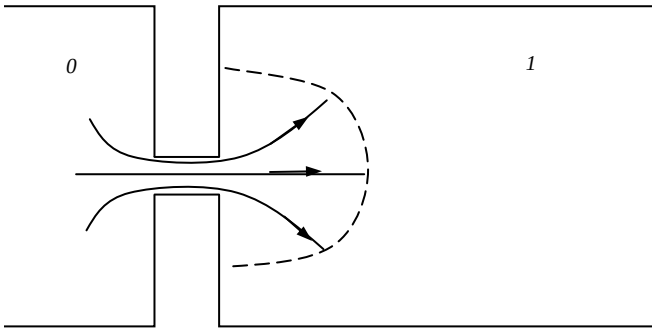

Fig. 2 The gas flow from the gas attenuator to the first stage of the differential pumping system. Arrows mark streamlines. Dashed line is a shock front separating cold supersonic gas to the left of the front and the room-temperature shocked gas to the right.

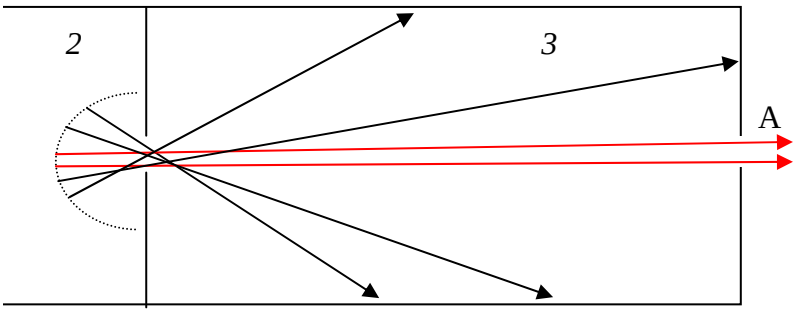

Fig. 3. Towards evaluation of the beam particle flux. The dotted hemisphere with the radius of the order of particle mean free path in cell 2 depicts the area where the flow becomes collisionless. At this surface the particles have an isotropic distribution. Only the particles whose velocity vectors lie in a very narrow solid angle subtended by the exit orifice A escape directly to the undulator volume forming a beam. Two trajectories of such particles are shown in red. A vast majority of the particles (black arrows) move along trajectories hitting the walls of cell 3.